Applied Catalysis B: Environmental 132–133 (2013) 332–341

Contents lists available at SciVerse ScienceDirect

Applied Catalysis B: Environmental

journal homepage: www.elsevier.com/locate/apcatb

A novel BiOCl thin film prepared by electrochemical method and its application in photocatalysis

Xiaochao Zhang, Xiaoxia Liu, Caimei Fan*, Yawen Wang, Yunfang Wang, Zhenhai Liang

College of Chemistry and Chemical Engineering, Taiyuan University of Technology, Taiyuan 030024, PR China

ARTICLE INFO

Article history:
Received 17 August 2012
Received in revised form 3 December 2012
Accepted 9 December 2012
Available online 20 December 2012

Keywords:
BiOCl thin film
Electrochemical method
Photocatalysis
Methyl orange

ABSTRACT

In this study, a novel BiOCl thin film with flakelike structures has been successfully prepared through electrochemical method composed of a cathodic electrodeposition and an anodic oxidation at room temperature. The samples obtained at the different oxidation voltages were analyzed by X-ray diffraction (XRD), scanning electron microscope (SEM), electronic energy spectrum (EDS), and UV–vis diffuse reflectance spectra (UV–vis DRS). The analysis results show that the morphological, structural, and optical characteristics of BiOCl thin films depend markedly on the anode oxidation voltage and the lattice orientation of BiOCl thin film is transformed mainly into (1 1 0) surface with the increasing oxidation voltages. The observed results of high-resolution transmission electron microscopy (HRTEM) confirm that pure tetragonal BiOCl thin film with the highly exposed (1 1 0) surface is obtained at 2.0 V and consists of interlaced nanosheets. First-principles calculations reveal that the existence of BiOCl (1 1 0) surface states enhances the electron transition and efficient separation of photo-induced electron–hole pairs. The optimized BiOCl thin film can not only guarantee the intrinsic photochemical properties of BiOCl bulk but also exhibit additional electronic characteristics of BiOCl (1 1 0) surface, and consequently the wonderful synergistic effect between BiOCl bulk and BiOCl (1 1 0) surface accelerates the efficient separation of electron–hole pairs and produces the high reducing superoxide radicals $O_2^{-\bullet}$ and strong oxidizing hydroxyl radicals •OH required for the degradation of organic compounds. For as-prepared BiOCl thin film, the degradation ratio of methyl orange (MO) reaches 98% under 2.5 h UV irradiation at the first cycle and still remains 90% at the fifth cycle, and the COD removal efficiency of 50 mg/L MO solution over BiOCl thin film achieves 73.47% after 8 h reaction time. The BiOCl thin film with highly exposed {1 1 0} facets exhibits the excellent photocatalytic performance and potential application in photocatalysis field.

1. Introduction

Since Fujishima and Honda [1] discovered the photocatalytic splitting of water on TiO_2 electrodes in 1972, heterogeneous photocatalysis through semiconductor solid systems has become an exciting and rapidly growing research area in developing several industrially oriented applications in the last few years [2]. Photochemical materials which used to be solid semiconductors could be excited via light energy higher than their band gaps, inducing the formation of energy-rich electron–hole pairs, and consequently, decomposing organics in water or air into CO_2 and H_2O through the generated active species (e.g. $O_2^{-\bullet}$, •OH) in the photo-induced processes [3]. Recently, Bismuth oxychloride, BiOCl, as one of the most intensively studied photochemical materials, has drawn considerable attention for promising practical industrial application due to its characteristic hierarchical structure and optical property as well as higher photocatalytic activity and stability [4–7]. For BiOCl with layered structure, there is the formed internal electric field between $[Bi_2O_2]^{2+}$ positive layer and negative Cl^- layer, which provides a large enough space to polarize the related atoms and orbitals, and consequently, improving the separation efficiency of photo-induced electron–hole pairs. More important thing is that BiOCl has an indirect transition band gap of 3.05–3.55 eV [8–11], so that it is necessary for photo-excited electrons to be emitted to valence band by a certain *k*-space distance, which reduces the recombination probability of photo-excited electrons and holes [12]. Therefore the special layer structure and indirect transition characteristic would help to enhance the electron–hole separation and charge transport of BiOCl photocatalyst, resulting in that BiOCl exhibited more stable and wonderful photocatalytic performance on the degradation of organic compounds than TiO_2 (P25, Degussa) [8,13–15]. For instance, Zhang et al. [8] firstly reported that BiOCl exhibited better photocatalytic activity than P25 at three-cycles for decomposing methyl orange

* Corresponding author. Tel.: +86 351 6018193/13007011210; fax: +86 351 6018554.
E-mail addresses: zhang13598124761@163.com (X. Zhang), fancm@163.com (C. Fan).

0926-3373/$ – see front matter © 2012 Elsevier B.V. All rights reserved.
http://dx.doi.org/10.1016/j.apcatb.2012.12.010

(MO) under ultraviolet (UV) light irradiation in 2006, and discussed the electronic structure of BiOCl using first-principles calculations based on density functional theory (DFT). Their results indicated that the open crystal structure and indirect optical transition of BiOCl played crucial roles in its excellent photocatalytic activity. Soon, An et al. [14] and Zhang et al. [15] reported that BiOCl showed outstanding photocatalytic activity on the degradation of Rhodamine B (RhB) and MO dyes under UV–visible light irradiation.

Recently, our group adopted a facile method to synthesize BiOCl photocatalyst that demonstrated higher photocatalytic activity than P25 under Xenon lamp and sunlight irradiation [10,16]. In order to obtain the precise nature of electronic transition properties, we further investigated the structural, electronic and optical properties of BiOCl with or without oxygen vacancy using first-principles method based on DFT in detail [17,18]. Our calculated results are in good agreement with our experiment data and the reported results of Zan et al. [12]. Up to now, the preparation technology of BiOCl powder samples was mainly divided into two kinds: hydrolysis method and solvothermal method. For example, Chang et al. [19,20] prepared BiOX(X = Cl, Br, I) photocatalysts via hydrolysis method using $NaBiO_3$ as raw material and evaluated their photocatalytic activities under Xenon lamp irradiation using pentachlorophenol–Na (PCP–Na) as target pollutant. Besides, our previous work also confirmed that as-prepared BiOCl [10] exhibited better photocatalytic activity via simple hydrolysis method using $BiCl_3$ as raw material. On the other hand, Zhu et al. [9] synthesized 3D hierarchitectures BiOCl by a template-free solvothermal method using $BiCl_3{\cdot}5H_2O$ as raw material and glycol as solvent, and Chen et al. [21] adopted the same preparation technology to obtain BiOCl photocatalyst with excellent photocatalytic activity for decomposing MO and RhB under UV light irradiation. According to the previous reported results, it is found that BiOCl is biologically and chemically inert, stable to corrosion, non-toxic and relatively inexpensive. Thus BiOCl would become a competitive and promising photochemical material in the photocatalytic application field.

Take a panoramic view of the previous achievements, most of investigations have focused on the synthesis and characterization of BiOCl nanopowder samples as well as BiOCl photo-response modifications including photosensitizer responding (such as Bi_2O_3/BiOCl [22], WO_3/BiOCl [23], Bi_2S_3/BiOCl [24]), semiconductor compounding (Fe_3O_4/BiOCl [25], BiOCl/Bi_3O_4Cl [26], Bi_2O_3/BiOCl/WO_3 [27], $Bi(OH)_3$/BiOCl [28], BiOI/BiOCl [29], Ag_3PO_4/BiOCl [30], etc.), noble metal loading [31], nonmetal [32,33] or transition metal doping [34,35]. As is well known, the nanoparticle suspension photocatalysts with high surface areas are advantageous for the adsorption of organic pollutants on the surface of catalysts and the next oxidation–reduction reaction. Nevertheless, the nanopowder photocatalysts possess several defects such as rather difficult to be separated from solution and be recycled, easy aggregation and potential risks for humans. Therefore, the immobilized BiOCl thin film with good phtocatalytic activity should indicate a promising industrial application in the effective remediation of environmental pollution such as water or air pollutants treatment [4,36–38]. Cao et al. [37] reported a novel BiOCl film with flowerlike hierarchical structure fabricated by dipping Bi film in a mixed solution of H_2O_2 and HCl for the first time, indicating its potential application in optoelectronic device, but have not provided the relative study on the photocatalytic performance of BiOCl film. Recently, Wu et al. [4] prepared BiOCl nanowire arrays via employing the anodic aluminum oxide (AAO) template assisted sol–gel method, and confirmed the higher photocatalytic activity for decomposing Rh B under UV irradiation, but their study did not explore systematically the relationship between intrinsic structural characteristic and photocatalytic property of immobilized BiOCl photocatalyst.

In order to investigate the immobilization of BiOCl and photocatalytic activity of immobilized BiOCl thin film, our laboratory has successfully prepared the BiOCl thin film with flowerlike sphere structure on Ti substrate by an alcoholysis-coating method using $BiCl_3$ as precursor at low temperatures, and interestingly the as-prepared thin film exhibited excellent photocatalytic performance [38]. These results strengthen our confidence to pursue better immobilized method of BiOCl thin film, and it is expected to further establish and study the relationships among the intrinsic structural property, photocatalytic activity, degradation mechanism and immobilization method so as to overcome the problem of solid–liquid separation and eliminate the practical barriers of photocatalytic technology. This work is meaningful for the final realization of the photocatalytic degradation of toxic recalcitrant organic pollutants in environment by utilizing the solar energy.

In this article, we have successfully prepared the BiOCl thin films at room temperature by a novel electrochemical method composed of a cathodic electrodeposition and an anodic oxidation, which is both energy-saving and environment-friendliness. The as-prepared BiOCl thin films are analyzed by X-ray diffraction (XRD), scanning electron microscope (SEM), electronic energy spectrum (EDS), UV–vis diffuse reflectance spectra (UV–vis DRS) and High-resolution TEM (HRTEM). The well-crystalline BiOCl thin film with exposed {1 1 0} facets possesses superior photocatalytic activity and stability. Furthermore, we explore the influences of the preparation conditions and structural properties on photocatalytic activity of BiOCl thin film. Finally, the band structure and electronic density of states for the immobilized BiOCl thin film are discussed by the first-principles calculation based on DFT, to further describe the possible photocatalytic mechanisms and charge carrier transition characteristics. Our results should provide a good foundation for the investigations on the relationships between the surface engineering and the photocatalytic properties of BiOCl thin film, and push on the progress in its actual application in photoctalytic field.

2. Experimental

2.1. Pretreatment of Ti substrates

Ti substrates (80 mm × 10 mm × 2 mm) were burnished using abrasive paper, and then surface-treated at 90 °C for 3 h in 10% (quality ratio) oxalic acid solution. Subsequently, Ti substrates were placed into 10% HCl solution for 3 h. The treated Ti substrates were cleaned using distilled water, after that they were stored in acetone solvent to avoid contact with air oxidation.

2.2. Preparation of BiOCl films

The preparation process of immobilized BiOCl thin film on Ti substrate mainly included two steps: the cathodic electrodeposition of Bi film on the Ti substrate and subsequently anodic oxidation of the Bi film into BiOCl thin film. The schematic preparation process for BiOCl thin film has been shown in Fig. 1. Firstly, the cathodic deposition of Bi film named Film 1 on a proper cleaned Ti substrate acted as the cathode was carried out in an aqueous solution of 0.006 M $Bi(NO_3)_3$ employing 3 mA cm^{-2} current density and Pt electrode as the anode. The pH value of working solution was 1 adjusted by HCl solution and the deposition process was completed at room temperature for 8 h. Secondly, the anodic oxidation process was performed in a two-electrode system at room temperature for 1 h under magnetic stir to form BiOCl film on Ti substrate, where the graphite electrode, obtained Film 1 and 3 wt.% NaCl aqueous solution were used as the cathode, anode and electrolyte, respectively. Then, a series of oxidation voltage of 1.5, 1.7, 2.0 and 2.5 V

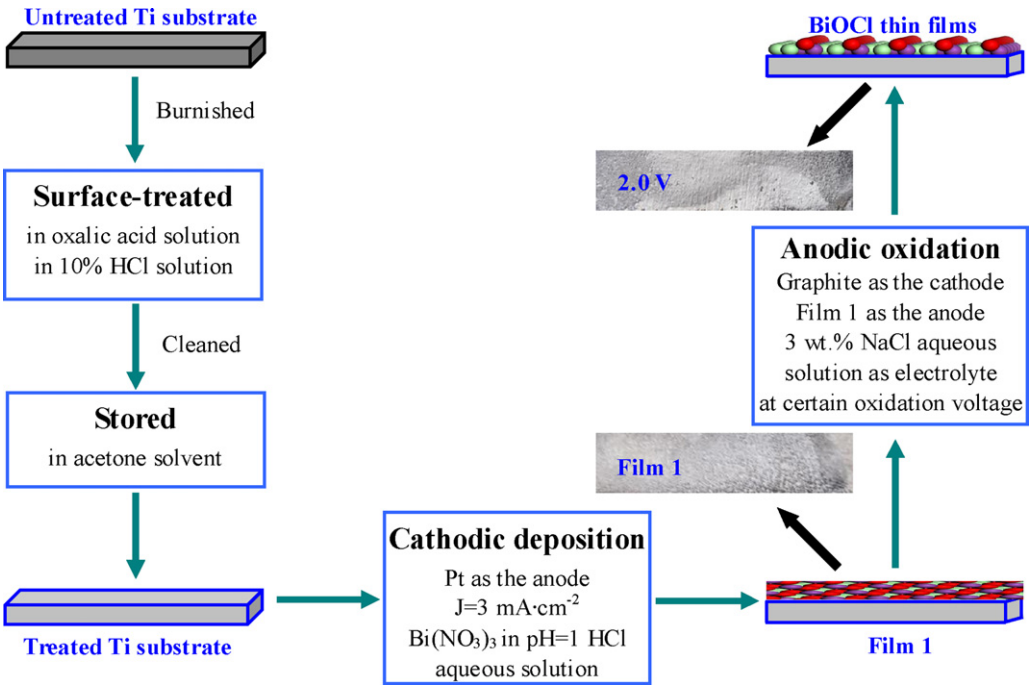

Fig. 1. The schematic of preparation process for BiOCl thin films.

were investigated to obtain the optimized oxidation voltage. The as-prepared BiOCl thin film was cleaned by distilled water and dried naturally in air at room temperature.

2.3. Characterization

The X-ray diffraction (XRD) analysis of BiOCl thin film on Ti substrate was carried out using a D/max-2500 diffractometer at a voltage of 40 kV and a current of 100 mA with Cu Kα radiation (λ = 0.15418 nm) across a 2θ range 5°–70°, at a scan rate of 8° (2θ)/min, determining the identity of any phase present and their crystallite sizes. The morphology and thickness of BiOCl thin film on Ti substrate were observed using a Nanosem430 field emission scanning electron microscope (FESEM) with an accelerating voltage of 15 kV. Elemental analysis of BiOCl thin film was accomplished by energy dispersive spectrometry (EDS) attached to FESEM. Transmission electron microscope (TEM) and high-resolution TEM (HRTEM) images were acquired using a JEOL JEM-2100 instrument working at an acceleration voltage of 200 kV. The UV–vis absorption spectra were examined on a Varian Cary 300 spectrometer.

2.4. Photocatalytic activity measurement

The photocatalytic activities of BiOCl thin film on Ti substrate was evaluated through the degradation of 10 mg/L methyl orange (MO) in water. In a typical photocatalytic experiment, the immobilized BiOCl thin film was hung in a cylindrical quartz glass reactor with an effective vessel volume of 50 mL MO solution, and a 250 W ultraviolet lamp with a main emission wavelength of 365 nm or a 500 W Xenon arc lamp (simulated sunlight) with a refrigerating water circuit acted as a slide light source, meanwhile, MO solution was aerated by air (the air velocity is 4.2 L/min) through a min-type pump to maintain the solution in agitation state. At given intervals of illumination, the samples of reaction solution were taken out and analyzed using a UV–vis spectrometer (VARIAN CARY 50Probe). The degradation efficiency (D) of MO was calculated by the following formula:

$$D = \frac{c_0 - c_t}{c_0} \times 100\% \quad (1)$$

where c_0 and c_t were the initial concentration (10 mg/L) and degradation concentration of MO during the photocatalytic degradation reaction, respectively.

The mineralization of MO was assessed via the decrease of chemical oxygen demand (COD) of dye solution. COD value was measured on the basis of the standard dichromate titration method [39]. The mineralization efficiency of MO was estimated by the following expression:

$$\text{Mineralization rate of MO } (\%) = \frac{\text{COD}_0 - \text{COD}_t}{\text{COD}_0} \times 100 \quad (2)$$

where COD_0 and COD_t is the COD concentration after 30 min adsorption–desorption equilibrium and COD concentration at certain reaction time t (h), respectively.

2.5. First-principles calculation

In this study, first-principles calculation was carried out using the well-tested Cambridge Serial Total Energy Package (CASTEP) code based on density functional theory (DFT) [40]. The exchange-correlation potential was described with the generalized gradient approximation (GGA) in the scheme of Perdew–Burke–Ernzerhof (PBE) [41]. For an investigation on the electronic structure and ground-state property, the valence electronic configurations are Bi-$6s^2 6p^3$, O-$2s^2 2p^4$ and Cl-$3s^2 3p^5$ states. The Kohn–Sham wave function of valence electrons was expanded in plane-wave within a cutoff energy of 340 eV. The Brillouin zone integrations were approximated using a $3 \times 3 \times 3$ k-point grid sampling scheme of Monkhorst–Pack [42]. To further obtain reasonable results, the lattice parameters of BiOCl crystal were firstly optimized by an iterative process, obtaining the bulk structure equilibrium. In the iterative process, the maximum root–mean–square convergent tolerance is less than 1×10^{-6} eV/atom; the force imposed on each atom is not greater than 0.1 eV/nm and a stress of less than 0.05 GPa.

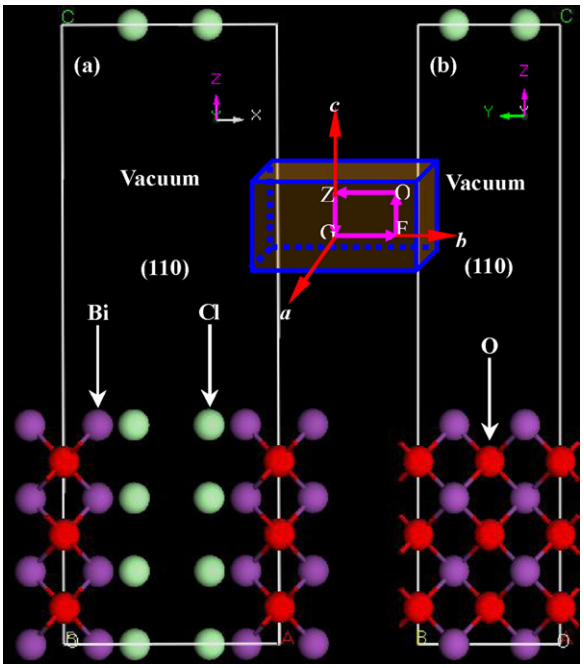

Fig. 2. Geometry models for the (1 1 0) surfaces of BiOCl based on a 22-atom slab structure with the vacuum thickness of 150 nm, hereinto, (a) and (b) represent the front view and side view of (1 1 0) surface, respectively (inset: the diagram of Brillouin Zone for calculating the electronic band structures of BiOCl bulk and (1 1 0) surface).

Then, BiOCl (1 1 0) surface was built from direct bulk cleavage as shown in Fig. 2, and thus exhibited undercoordinated atoms relative to BiOCl bulk structure. For BiOCl (1 1 0) surface with a sufficient vacuum thickness of 15 Å, all the atomic relaxations were performed at constant volume (at the bulk equilibrium lattice parameters) by using the conjugate gradient optimization scheme. Finally, based on the appropriate Brillouin zone integrations of periodic functions (the diagram of Brillouin zone inset in Fig. 2), the electronic structures of the optimized BiOCl bulk and relaxed (1 1 0) surface were calculated and further discussed in detail.

3. Results and discussion

3.1. Phase structure and morphology analysis of as-prepared samples

Fig. 3(a) presents the XRD patterns of as-prepared samples after anode oxidation at the oxidation voltages of 0 (Film 1), 1.5, 1.7 and 2.0 V for 1 h. Compared with pure tetragonal BiOCl [JCPDS file No. 06-0249] seen in Fig. 3(b), the characteristic peaks of BiOCl thin films at 0, 1.5 and 1.7 V exhibit the diffraction peaks of tetragonal BiOCl, but some diffraction peaks of Bi impurity [JCPDS file No.44-1246] are detected from the patterns of the thin films. The intensity of the Bi impurity peaks deceases gradually with the increase of oxidation voltage, which indicates that the larger oxidation voltage may be favorable to the transformation from Bi impurity into BiOCl. It is found that the intensity of characteristic (1 1 0) peak for {1 1 0} facets becomes relatively more remarkable than (1 0 1) and (1 0 2) characteristic peaks as well as {0 0 1} facets family such as (0 0 1), (0 0 2), and (0 0 3) with the increase of oxidation voltage. The strong (1 1 0) peak corresponds to the (1 1 0) plane [13,43], which suggests that the synthesis of BiOCl thin film with high percentage of exposed {1 1 0} facets, especially (1 1 0) planes, should be controlled through regulating oxidation voltage in the preparation process. When the oxidation voltage is 2.0 V, there is no Bi impurity phase detected and the intensity of characteristic (1 1 0) peak from XRD pattern of BiOCl is the most outstanding as shown in Fig. 3(b). By further observation from Fig. 3(b), the intensity ratios of (1 1 0) to (0 0 1), (0 0 2) and (0 0 3) for BiOCl are 7.06, 12.3 and 13.4, respectively, which are clearly higher than the standard ratios of 1.88, 4.69 and 6.25, and ones of (2 2 0) to (0 0 1), (0 0 2) and (0 0 3) are 1.54, 2.67 and 2.90 obviously higher than the standard ratios of 0.3, 0.75 and 1. Thus, for the initial formation of BiOCl crystal, the growth orientation of BiOCl microcrystals is in the longitudinal direction, that is, the growth direction is (0 0 1), because {0 0 1}–1Cl facets of BiOCl possesses the lowest cleavage energy of 0.026 J/m^2, while the {0 0 1}–2Cl and {0 0 1}–BiO have the highest value of 2.349 J/m^2. With the increasing oxidation voltage, the side facets of BiOCl nanoflakes are composed of the (1 1 0) family of planes (1.426 J/m^2) and other planes [13,44]. The results show that the facades of as-prepared tetragonal BiOCl thin film at 2.0 V should be dominated by {1 1 0} facets, especially (1 1 0) surface, while the facades of the tetragonal BiOCl should be nearly enclosed by {0 0 1} facets [45].

The scanning electron microscope (SEM) images of the Ti substrate and BiOCl thin films obtained at the different oxidation voltages have been shown in Fig. 4. Fig. 4(a) displays the pretty rugged surface of treated Ti substrate, and lots of large particles adhere to the surface of Ti substrate forming Film 1 as shown in Fig. 4(b). It can be clearly seen that the obtained BiOCl thin film after anode oxidation at 1.5 V looks like "dry land" with several cracks and is more homogeneous than Film 1 as displayed in Fig. 4(c). With the increase of anode oxidation voltage, the as-prepared BiOCl thin films become more and more homogeneous and ordered array with the interlaced nanosheets keeping the same growth direction. Furthermore, abundant pores have been introduced into BiOCl thin film due to the staggered arrangement of BiOCl nanosheets, which will increase the specific surface area of BiOCl thin film Fig. 4(d) and (e). By careful observation, it can be seen that the as-prepared BiOCl thin film at 2.0 V exhibits the well-ordered nanoplates with rather smaller size and better compact arrange seen as Fig. 4(e). Additionally, the EDS spectrum of BiOCl thin film obtained at 2.0 V has been plotted in Fig. 4(f). There are Bi, O and Cl elements in the EDS spectrum of BiOCl thin film, and the quantitative analysis result of which demonstrates that the value of Bi:O:Cl (in quality) is 78.45:4.18:13.37, close to the stoichiometric ratio of BiOCl (80.23:6.14:13.62). The obtained results are in good consistent with the reported findings of Cao et al. [46]. To further confirm the sheet-shaped structure, well-crystallized and growth orientation of BiOCl thin film obtained at 2.0 V, the corresponding transmission electron microscope (TEM), high-resolution TEM (HRTEM) micrographs and selected area electron diffraction (SAED) pattern taken from an individual sheet have been acquired and represented in Fig. 5. The TEM micrograph (Fig. 5(a)) shows the several BiOCl ultrathin nanoplates with a width of about 50–100 nm and thickness of 30 nm. The HRTEM micrograph (Fig. 5(c)) reveals clearly the lattice fringes with a lattice spacing of 0.275 nm that is consistent with the (1 1 0) and (1 $\bar{1}$ 0) planes of the tetragonal system of BiOCl, while the right corner of HRTEM appears the lattice spacing of 0.75 nm that agrees well with the spacing of the tetragonal BiOCl (0 0 1) planes, which confirm that as-prepared BiOCl thin film at 2.0 V mainly consists of nanosheets stacked together along the *c*-axis [47]. According to the above discussions and the geometry symmetry of tetragonal BiOCl, the growth tendency of BiOCl thin film as a function of oxidation voltages (0–2.0 V) is gradually parallel to the *c*-axis along [0 0 1] direction, resulting in the higher percentage of {1 1 0 } facets, as shown in Fig. 5(b). Furthermore, it can be seen clearly from the inset of Fig. 5(c), the angle labeled in the corresponding FFT pattern is 90°, which is identical to the theoretical value for the angle between (1 1 0) and (1 $\bar{1}$ 0) planes and the previously experimental results [13,28,32,43,47–48]. Our results indicate that the well-crystallized tetragonal BiOCl thin film with highly exposed

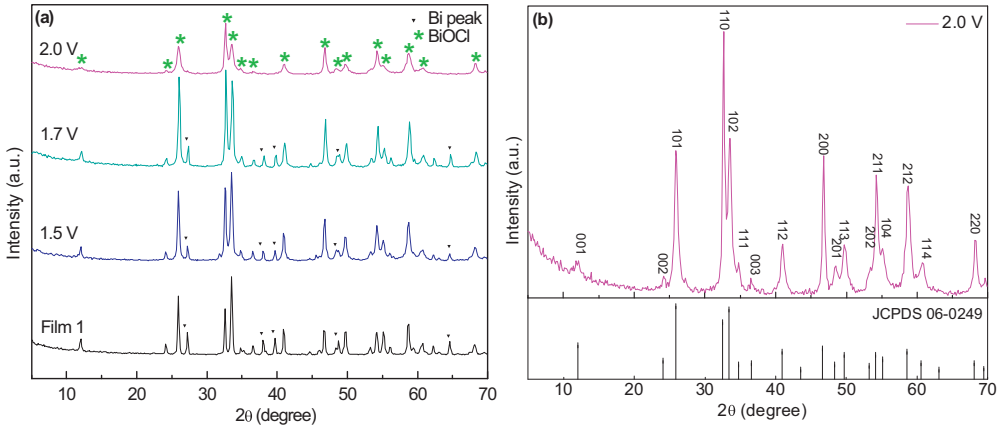

Fig. 3. XRD spectra of as-prepared BiOCl thin films: (a) XRD spectra of as-prepared BiOCl thin films obtained at different oxidation voltage, (b) the amplified XRD spectrum of BiOCl thin film at 2.0 V and the standard XRD peaks of the tetragonal BiOCl structure (JCPDS 06-0249).

{1 1 0} facets can be synthesized by the cathodic electrodeposition and anodic oxidation method at room temperature.

3.2. *Effect of anode oxidation voltage on photocatalytic activities of BiOCl thin films*

It is well known that photocatalytic activity of semiconductor photocatalyst has been relative to its band gap, grain size, morphology, surface property, electronic structure, and so on [49]. However, BiOCl photocatalyst, as one kind of indirect band gap semiconductor materials, has been proved to have more stable and wonderful photocatalytic performance than P25 on the degradation of organic compounds [8,13–15], but little information on the relevancies among microstructure properties, photocatalytic activity and stability of BiOCl thin film has been reported and discussed. Thus it is necessary for us to make a relatively comparative study of microstructure properties such as band gap, surface property, electronic structure, etc., photocatalytic activity and stability of the BiOCl thin films obtained after anode oxidation at the different voltages so as to determine the optimal oxidation voltage in our experiments. Fig. 6 shows the degradation efficiencies of MO by BiOCl thin films obtained at the various anode oxidation voltages as a function of UV illumination time and the photos of them. Since the Film 1 has no photocatalytic activity and the BiOCl

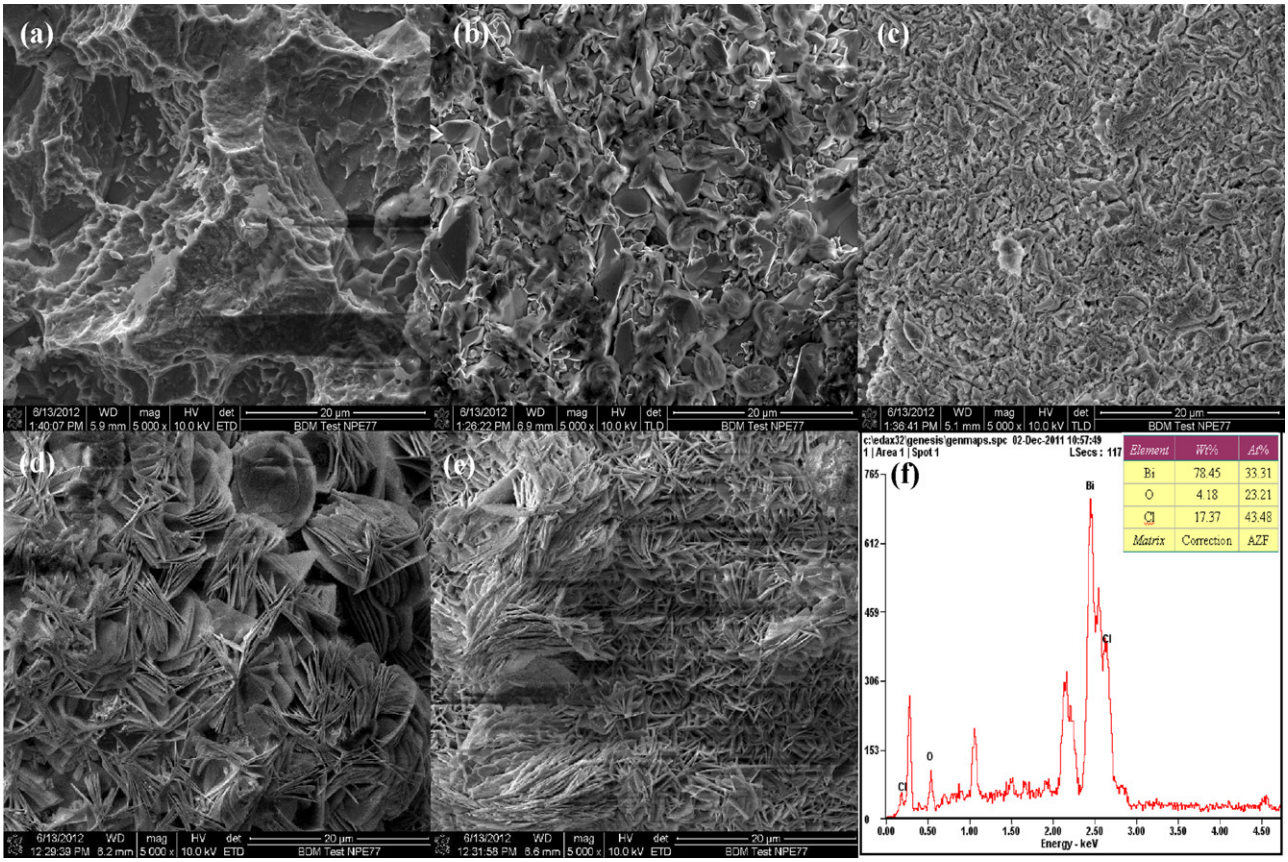

Fig. 4. SEM images of treated Ti substrate (a) and BiOCl thin films at the oxidation voltages of 0 V (b), 1.5 V (c), 1.7 V (d) and 2.0 V (e) as well as the EDS spectrum of BiOCl thin film at 2.0 V (f).

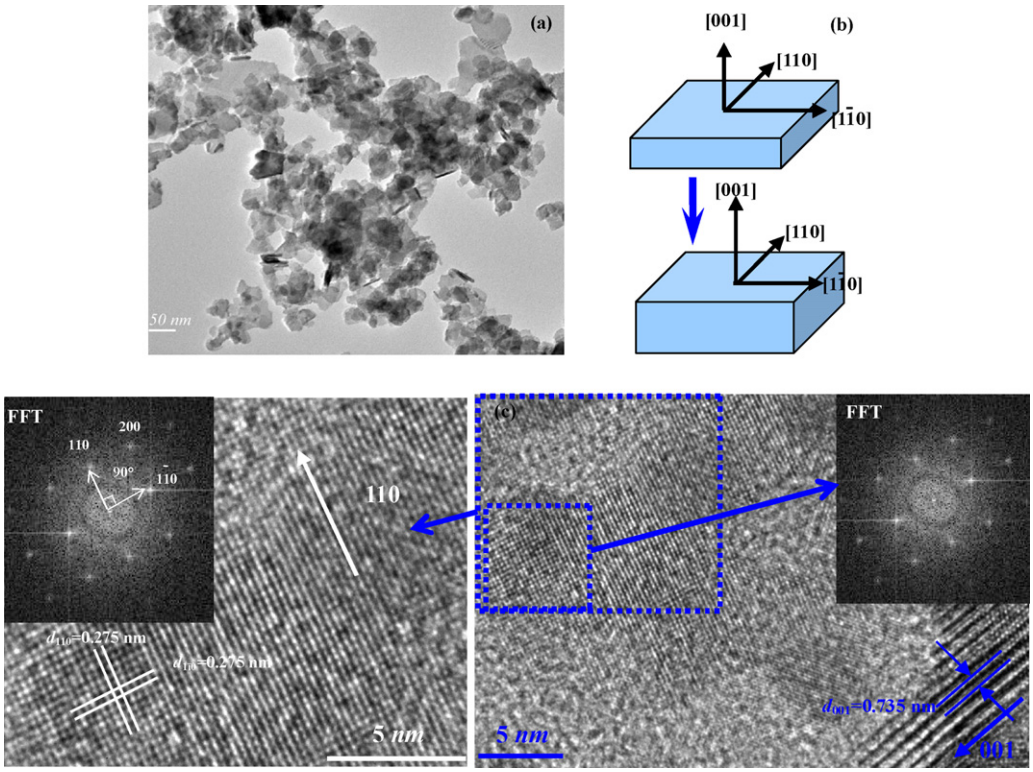

Fig. 5. (a) Low-resolution TEM image of BiOCl thin film obtained at 2.0 V, (b) the growth tendency of BiOCl thin film as a function of oxidation voltages (0–2.0 V), (c) corresponding high-resolution TEM (HRTEM) micrograph and selected area electron diffraction (SAED) pattern taken from an individual sheet.

thin film at 2.5 V easily falls off from Ti substrate, the results about Film 1 and BiOCl thin film at 2.5 V are not listed here. According to the experimental results from Fig. 6, the as-prepared BiOCl thin films at 1.5, 1.7 and 2.0 V reveal the significant degradation efficiencies of MO as a function of UV illumination time. After 2.5 h under UV irradiation, the decomposed rates of MO aqueous solution are 81%, 90% and 98%, respectively, indicating that anode oxidation voltage is one of the most important factors to affect the photocatalytic activity of BiOCl thin film. As aforementioned, the intensity of characteristic peaks for {1 1 0} facets, especially (1 1 0) crystal plane, becomes more obvious than that for others by controlling the anode oxidation voltage in the preparation process, and the morphology structure of as-prepared BiOCl intensively depends on the anode oxidation voltage value, suggesting that the best photocatalytic activity of BiOCl thin film at 2.0 V should be closely related to the higher percent of (1 1 0) surface and perfect morphology structure. What is more, there are possible reasons explained as follows: (1) compared with pure tetragonal phase BiOCl thin film at 2.0 V, thin films at 1.5 and 1.7 V are composed of the mixture of Bi impurity and tetragonal BiOCl phase that maybe affect their absorption ability to some extent; (2) according to the Scherrer formula that the wider full width at half maximum (FWHM) of the strongest peak, the smaller grain size of particle. Thus BiOCl thin film at 2.0 V exhibits the smallest grain size, simultaneously the nanoplates of thin film arrange more compact, which should increase its superficial area and improve its photocatalytic activity; (3) with the increasing anode oxidation voltage, the catalyst amount deposited on the surface of Ti substrate gradually becomes more and more, obtaining the optimized amount up to 2.0 V, over which the color and immobilization strength will vary significantly by observing the photos of the as-prepared samples as inset in Fig. 6. The color of thin films changes obviously from gray (2.0 V) to white (2.5 V), and the white thin film is not stable and easily falls from Ti substrate during the anode oxidation process in our experiments, this is the major reason why the photocatalytic activity of BiOCl thin film over 2.5 V has been not investigated. In sum, based on the electrochemical method, the as-prepared BiOCl thin film with a higher exposed (1 1 0) surface exhibits the better photocatalytic performance. Most recently, Pare et al. [11] and Cui et al. [43] determined that the high photodegradation efficiency of BiOCl was associated with the atomic arrangement of its exposed {1 1 0} facets, but a relevant investigation on the electronic structure and surface property of {1 1 0} facets has been not carried out. Therefore, the obtained BiOCl thin film with the most prominent (1 1 0) crystal plane under the anode oxidation voltage value of 2.0 V, as the optimal oxidation voltage, should be further investigated and discussed in detail so as to explore the relationships among electronic structure, surface property, photocatalytic activity and mechanism.

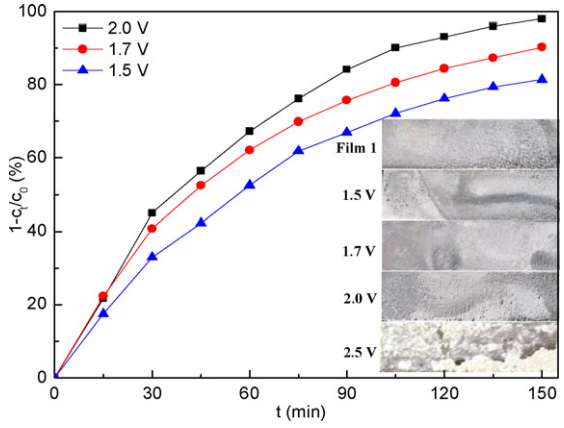

Fig. 6. Photocatalytic properties of BiOCl thin films at the oxidation voltages of 1.5, 1.7 and 2.0 V and the photos of the obtained thin films at the oxidation voltages of 0 (Film 1), 1.5, 1.7, 2.0 and 2.5 V.

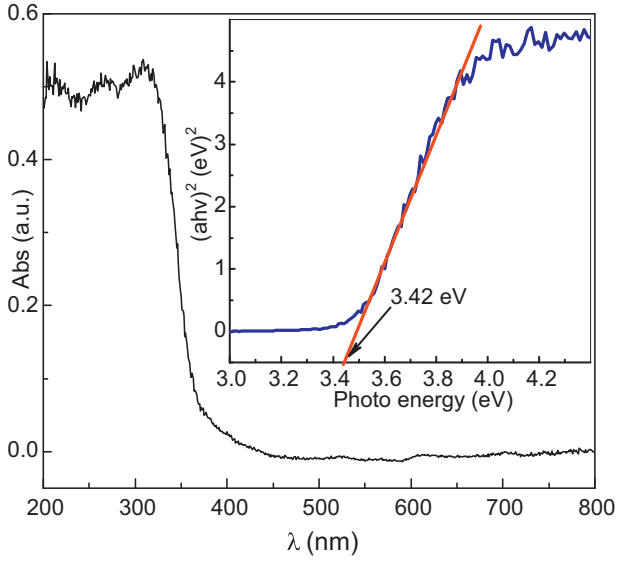

Fig. 7. UV–vis diffuse reflectance spectrum of BiOCl thin film at the oxidation voltages of 2.0 V (inset: plots of $(\alpha h\nu)^{1/2}$ versus photon energy ($h\nu$)).

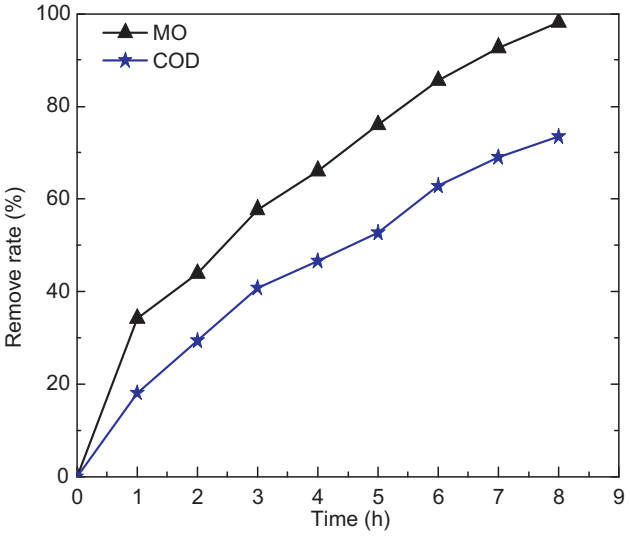

Fig. 9. Removal and mineralization rates of 50 mg/L MO solution over the as-prepared BiOCl thin film at 2.0 V during the photocatalytic reaction under UV light irradiation.

3.3. Photocatalytic activity and stability of optimized BiOCl thin film

To completely investigate the photocatalytic activity and stability of optimized BiOCl thin film, we consider the BiOCl thin film obtained under the optimal anode oxidation voltage value of 2.0 V as a unique research target. Firstly, the optical absorption property of BiOCl thin film is plotted in Fig. 7. The BiOCl thin film shows the favorable absorption property in the UV light area. According to the previous reported data, BiOCl is a kind of indirect band gap semiconductor and its band gap energy (E_g) is between 3.05 and 3.55 eV calculated by plotting $(\alpha h\nu)^2$ versus photon energy $h\nu$ [8–11]. As inset in Fig. 7, our calculated E_g value of 3.42 eV for the BiOCl thin film is coincident with the previous calculated values.

The photocatalytic activity of BiOCl thin film at 2.0 V is further evaluated by the degradation of MO under UV light irradiation. Fig. 8 displays the UV–vis scanning curves of MO solution during the photocatalytic process. The strong absorption peak of MO

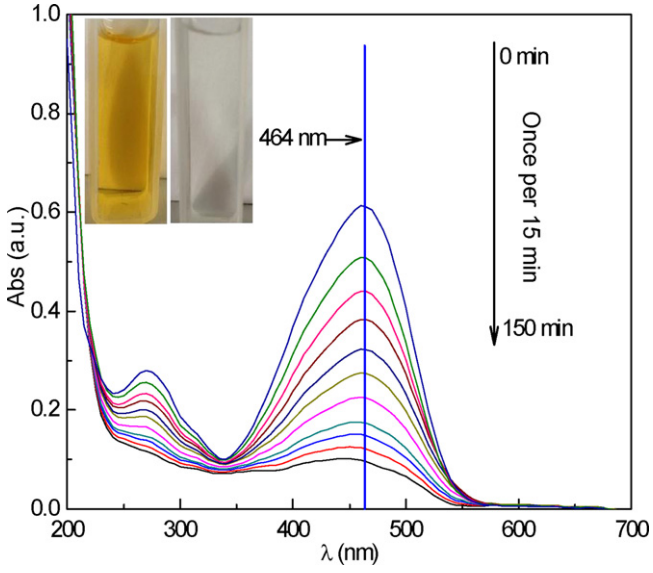

Fig. 8. Photocatalytic activity of BiOCl thin film at the oxidation voltages of 2.0 V.

solution detected at 464 nm gradually become lower and lower with the increase of photocatalytic reaction time, suggesting that MO should be gradually decomposed. It can be clearly seen that there is no other new absorption peak detected during the photocatalytic degradation process, and there is no maximum peak shift of MO, indicating that the self-photosensitization process cannot occur under these conditions [50]. Furthermore, the photos of MO solution before and after the photocatalytic degradation reaction have been inset in the upper-right corner of Fig. 8 for comparison. The color of MO solution disappears completely after 150 min. As well known, chemical oxygen demand (COD) value is used generally to determine the mineralization standard of organic compound and examine the water quality [51,52]. Fig. 9 shows that the associated COD removal test of 50 mg/L MO solution over as-prepared BiOCl thin film at 2.0 V during the photocatalytic reaction under UV light irradiation. It was observed that the COD removal rate increased with the increase of irradiation time, and 73.47% COD removal efficiency was achieved after 8 h reaction time over as-prepared BiOCl thin film at 2.0 V under UV light irradiation. Furthermore, considering the upward trend of the COD curve, longer irradiation is required in order to achieve the complete mineralization of MO. Additionally, it can be seen that the mineralization rate of MO is slower than the degradation rate of MO from Fig. 9, suggesting that the chromophore of MO molecular should be easily destructed for photocatalytic degradation of MO by the BiOCl thin film under UV light irradiation, and then the degradation intermediates with small molecular were further mineralized to CO_2 and H_2O.

In order to thoroughly clarify the roles of light and film catalyst as well as the cooperation of light and film catalyst, the corresponding experiments of photolysis, adsorption and photocatalysis have been designed and carried out during the degradation of MO as shown in Fig. 10. The results reveal that BiOCl thin film has a strong adsorption (50%) of MO dye under dark condition after 150 min. Without the existence of BiOCl thin film, the degradation rate of MO dye is only 17% after 150 min under UV irradiation, while the degradation rate of MO dye can reach 98% after 150 min under the cooperation of BiOCl thin film and UV light. Therefore, we make a conclusion that photocatalysis plays a key role in the degradation of MO dye under UV irradiation. In addition, under the simulated sunlight irradiation, MO can be slightly decomposed (about 63%) in

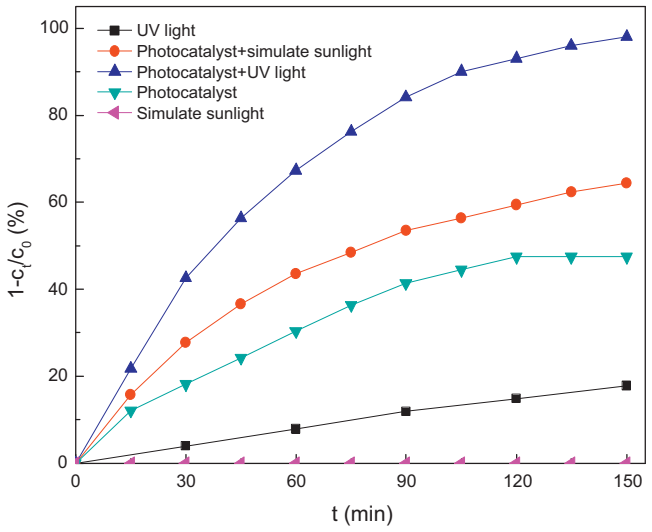

Fig. 10. Comparison of photolysis, adsorption and photocatalysis processes for the degradation of MO.

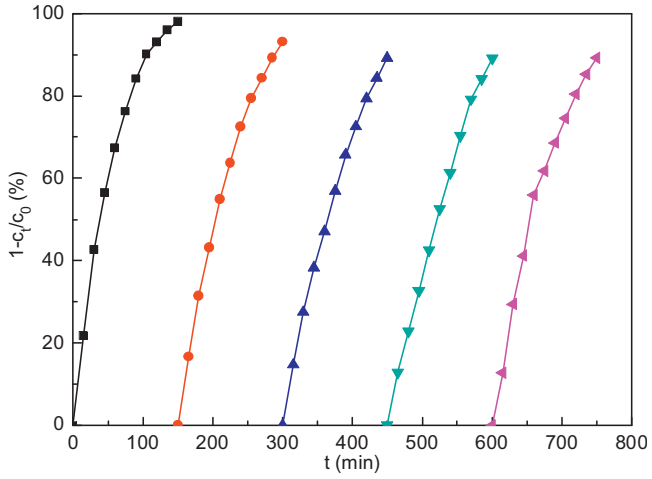

Fig. 11. Recyclability of BiOCl thin film at the oxidation voltages of 2.0 V.

the photocatalytic process, this maybe mainly attribute to the UV light existing in the simulated sunlight.

Compared with powder catalyst, the prominent advantage of immobilized thin film catalyst is that thin film catalyst can resolve the intractable problem of the complicated solid–liquid separation. As a photocatalystic material, the rather stabile activity is an all-important factor in the heterogeneous photocatalysis reaction system. Thus it is very necessary for us to perform the accelerated stability experiments so as to determine if the as-prepared BiOCl thin film possesses the recyclability under the photocatalytic reaction conditions. The used BiOCl thin film is only cleaned using distilled water after one cycle, and then dried in air for next cycle. The corresponding degradation results of MO solution for used BiOCl thin film reexamined for five cycles have been shown in Fig. 11. After the third cycle of repetition test for photocatalytic degradation of MO dye, BiOCl thin film exhibits no any significant loss of photocatalytic activity. The experimental results completely verify that as-synthesized BiOCl thin film should be provided with the more stable and excellent photocatalytic performance on degradation of MO dye.

3.4. Electronic band structure calculations

The electronic band structures of the optimized BiOCl bulk and relaxed (1 1 0) surface have been calculated and presented in Fig. 12 due to the as-synthesized BiOCl thin film existing the higher percent of (1 1 0) surface (the structure model and diagram of an appropriate Brillouin zone integrations of periodic functions in the calculated process for them have been described in Fig. 2). For BiOCl bulk, the calculated indirect band gap is 2.62 eV between the valence band maximum (VBM) of 0.0 eV at the *Z* point and conduction band minimum (CBM) near the *G* (or *Q*) point of 2.62 eV, which are in better agreement with the previous calculated data of 2.64 eV [17], 2.62 eV [35] by Fan et al., 2.60 eV [53] and 2.64 eV [54] by Huang and Zhu. The VBM is mainly contributed by the localized O 2p and Cl 3p states and the CBM by the unoccupied Bi 6p state. Compared with BiOCl bulk, the relaxed (1 1 0) BiOCl surface exhibits unique characteristics that the unoccupied Bi 6p state mainly appears from −0.89 to 0.66 eV and is much more dispersed in the entire CB part, and that the total density of states (TDOS) profile of relaxed BiOCl (1 1 0) surface shifts toward lower energy region seen as Fig. 12, which help to the electron transition and efficient separation of photo-induced electron and hole pairs

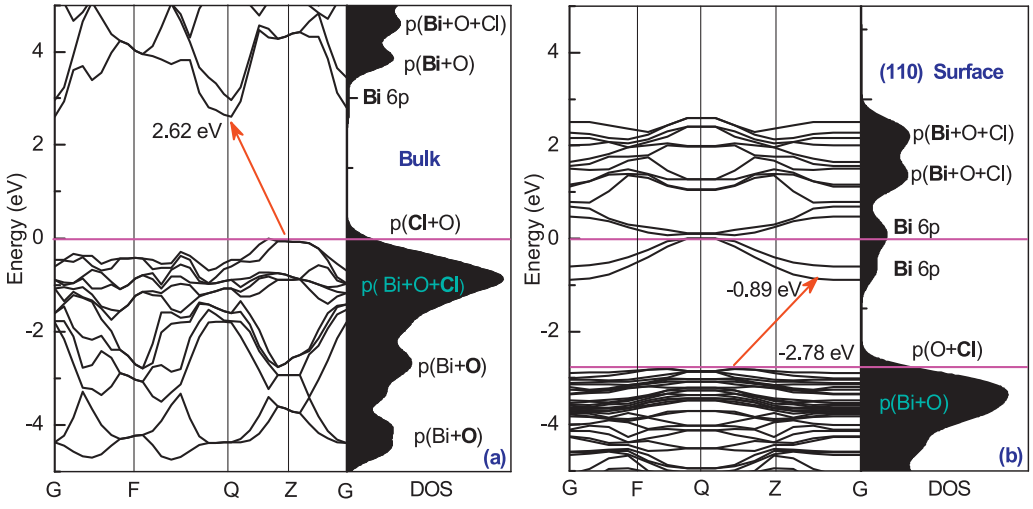

Fig. 12. Electronic band structures of optimized BiOCl bulk (a) and relaxed BiOCl (1 1 0) surface (b).

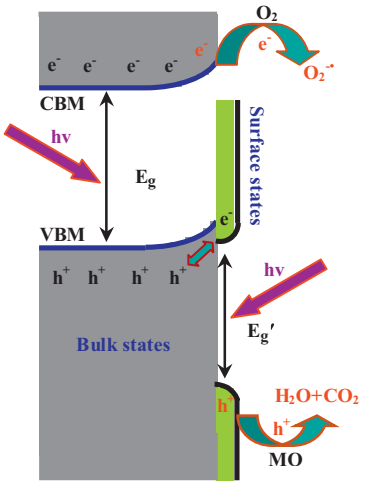

Fig. 13. Relative schematic diagram of possible synergistic mechanism process for electrons and holes transport between BiOCl bulk states and (1 1 0) surface states.

[17]. Furthermore, the electronic structures of them are both similar and different. For instance, their VBMs are mainly contributed by the O 2p and Cl 3p states, while CBM of relaxed BiOCl (1 1 0) surface reveals more and more unoccupied Bi 6p states that may be ascribed to the appearance of bismuth enrichment in the (1 1 0) surface structure (seen as Fig. 2). Therefore, the as-synthesized BiOCl thin film can not only guarantee the intrinsic photochemical properties of BiOCl bulk but also exhibit the additional electronic properties of BiOCl (1 1 0) surface, obtaining the interestingly synergistic effect between them.

3.5. Photocatalytic mechanism

Combined with the experimental analysis results and computational conclusions via first-principles method, the possible photocatalytic mechanisms have been discussed here. The relative schematic diagram of possible synergistic mechanism process for electrons and holes transport between the BiOCl bulk and BiOCl (1 1 0) surface has been plotted in Fig. 13. Generally, the DFT method underestimates band gap of semiconductor [55], and the absolute value of the calculated band gap is unreliable, but the relative value is feasible in the previous research [56]. Therefore, we can compare the differences in the band structures between the BiOCl bulk and BiOCl (1 1 0) surface. Through the comparison analysis of Fig. 13, the band gap of BiOCl (1 1 0) surface is narrower than that of BiOCl bulk, this is due to the energy levels near CBM and VBM originated from BiOCl (1 1 0) lattice-work structured surface Bi and Cl orbital by the analysis results of their electronic densities of states, respectively (seen as the exposed Bi and Cl atoms on the BiOCl (1 1 0) surface termination layer in Fig. 2). In the reported experiment, Chen et al. [21] found that accumulation of Bi^{3+} on the surface of BiOCl catalyst played a key role in enhancing the photocatalytic degradation of MO dye. The experimental results of Cui et al. [43] revealed that the synthesized BiOCl nanostructures with {1 1 0} facets could efficiently photodegrade MO dyes under either UV light irradiation or visible light irradiation because the atomic structure along {1 1 0} planes could generate local internal electrostatic field that benefits the separation of photo-induced electrons and holes under UV light irradiation, and the existence of exposed positive charged [Bi–Cl] layers on the surface of BiOCl solids facilitates the adsorption of MO dyes which promotes the photosensitization process under visible light irradiation. Furthermore, the surface states maybe partly affect the electronic transition due to the stronger ionic bonds between Bi and Cl atoms than that between Bi and O atoms for BiOCl semiconductor reported by our previous work [17,18]. Therefore, the efficient creation of electron–hole pairs for the present photochemical reaction can be mediated by the appearance of surface states in the BiOCl (1 1 0) lattice-work structure surface. Where, both BiOCl bulk and BiOCl (1 1 0) surface should achieve the electronic transition under UV light irradiation. The BiOCl (1 1 0) lattice-work structured surface has a surface state that penetrates into the bulk band gap, resulting in that the electrons (e^-) in the CBM of BiOCl (1 1 0) surface and holes (h^+) in the VBM of BiOCl bulk partly recombine, and consequently, obtaining the efficient electrons (e^-) and holes (h^+) located at the CBM of BiOCl bulk and VBM of BiOCl (1 1 0) lattice-work structured surface, respectively [56,57]. Finally, the efficient electrons (e^-) are easily transferred to oxygen molecule absorbed on the surface of BiOCl thin film to produce superoxide radicals $O_2^{-\bullet}$, and the efficient holes (h^+) react with H_2O to produce hydroxyl radicals $^\bullet$OH, achieving the indeed high reducing and strong oxidizing agents required for the degradation of MO dye, respectively, as displayed in Fig. 13. In addition, our experimental results confirmed that there is outstanding photocatalytic performance for the degradation of MO dye, and previous researches revealed that both superoxide radicals $O_2^{-\bullet}$ and hydroxyl radicals $^\bullet$OH played in very important roles in the photocatalytic degradation of MO dye for BiOCl photocatalytic material [7]. Therefore, our as-synthesized BiOCl thin film should realize the synergistic effect of $O_2^{-\bullet}$ produced by the electrons in the CBM of BiOCl bulk and $^\bullet$OH produced by the holes in the VBM of BiOCl (1 1 0) lattice-work structured surface, achieving the completely effective degradation of MO. Our experimental and theoretical results should be conducive to realize the immobilization of BiOCl photocatalyst as a promising candidate of photochemical material applied in the photocatalytic field, and further provide new insights into understanding the morphology control, electronic structure, surface property and facet-dependent photocatalytic property of BiOCl thin film.

4. Conclusion

A novel BiOCl thin film with nano-flakelike structures has been successfully prepared by a kind of electrochemical method containing a cathodic electrodeposition and an anodic oxidation at room temperature. The morphological, structural and optical characteristics of as-synthesized BiOCl thin films are found to depend markedly on the anode oxidation voltage on the basis of the analysis results of XRD, SEM, EDS, TEM, HRTEM, UV–vis, DRS, etc. The BiOCl thin films at the anode oxidation voltages of 1.5 and 1.7 V are composed of Bi impurity and tetragonal BiOCl phase, while pure tetragonal BiOCl thin film with the prominent (1 1 0) surface is obtained at 2.0 V and all staggered to distribute on the surface of Ti substrate. DFT results reveal that the unoccupied Bi 6p states of relaxed BiOCl (1 1 0) surface mainly appear near Fermi level of BiOCl bulk and disperse in the entire CB part, and that the TDOS profile of relaxed BiOCl (1 1 0) surface shifts toward the lower energy region, enhancing the charge carrier transition and efficient separation of photo-induced electron–hole pairs. The as-prepared BiOCl thin film at 2.0 V can not only guarantee the intrinsic photochemical properties of BiOCl bulk but also exhibit the additional electronic properties of BiOCl (1 1 0) surface, obtaining the wonderfully synergistic effect between them, and consequently, producing the high reducing superoxide radicals $O_2^{-\bullet}$ and strong oxidizing hydroxyl radicals $^\bullet$OH required for the degradation of organics and accelerating the efficient separation of electron–hole pairs. Thus as-prepared BiOCl thin film exhibits the excellent photocatalytic performance and perfect stability for the degradation of methyl orange (MO) under UV irradiation. The degradation ratio of MO reaches 98% at the first cycle and still remains 90% at the fifth cycle, and the

COD removal rate of 50 mg/L MO solution over BiOCl thin film achieves 73.47% after 8 h reaction time. In addition, this immobilization technology possesses the facile, simple, energy-saving and environmentally friendly advantages. Our findings could shed light on the further understanding of facet-dependent photoreactivity of BiOCl thin film and other new semiconductors, the fine manipulation of their photoreactivity as well as the progress of actual application for BiOCl photocatalytic material.

Acknowledgments

The authors gratefully acknowledge the financial support offered by the National Natural Science Foundation of China (21176168), International Cooperation Project of Shanxi Province (2012081017), and Science and Technology Project of Taiyuan, China (120123). We would express our great appreciation to Professor Peide Han for the technical help and useful discussion.

References

[1] A. Fujishima, K. Honda, Nature 238 (1972) 37–38.
[2] Z. Zou, J. Ye, K. Sayama, H. Arakawa, Nature 414 (2001) 625–627.
[3] A. Kubacka, M. Fernández-García, G. Colón, Chemical Reviews 112 (2012) 1555–1614.
[4] S.J. Wu, C. Wang, Y.F. Cui, T.M. Wang, B.B. Huang, X.Y. Zhang, X.Y. Qin, P. Brault, Materials Letters 64 (2010) 115–118.
[5] S.J. Wu, C. Wang, Y.F. Cui, W.C. Hao, T.M. Wang, P. Brault, Materials Letters 65 (2011) 1344–1347.
[6] C.H. Wang, X.T. Zhang, B. Yuan, C.L. Shao, Y.C. Liu, Micro & Nano Letters 7 (2012) 152–154.
[7] J. Jiang, K. Zhao, X.Y. Xiao, L.Z. Zhang, Journal of the American Chemical Society 134 (2012) 4473–4476.
[8] K.L. Zhang, C.M. Liu, F.Q. Huang, C. Zheng, W.D. Wang, Applied Catalysis B: Environmental 68 (2006) 125–129.
[9] L.P. Zhu, G.H. Liao, N.C. Bing, L.L. Wang, L.L. Wang, Y. Yang, H.Y. Xie, CrystEngComm 12 (2010) 3791–3796.
[10] Z.Q. Shi, Y. Wang, C.M. Fan, Y.F. Wang, G.Y. Ding, Transactions of Nonferrous Metals Society of China 21 (2011) 2254–2258.
[11] B. Pare, B. Sarwan, S.B. Jonnalagadda, Journal of Molecular Structure 1007 (2012) 196–202.
[12] L.Q. Ye, L. Zan, L.H. Tian, T.Y. Peng, J.J. Zhang, Chemical Communications 47 (2011) 6951–6953.
[13] K. Zhang, J. Liang, S. Wang, J. Liu, K.X. Ren, X. Zheng, H. Luo, Y.J. Peng, X. Zou, X. Bo, J.H. Li, X.B. Yu, Crystal Growth and Design 12 (2012) 793–803.
[14] H.Z. An, Y. Du, T.M. Wang, C. Wang, W.C. Hao, J.Y. Zhang, Rare Metals 27 (2008) 243–250.
[15] X. Zhang, Z.H. Ai, F.L. Jia, L.Z. Zhang, Journal of Physical Chemistry C 112 (2008) 747–753.
[16] Y. Wang, Z.Q. Shi, C.M. Fan, X.G. Hao, G.Y. Ding, Y.F. Wang, International Journal of Minerals Metallurgy and Materials 19 (2012) 467–472.
[17] X.C. Zhang, L.J. Zhao, C.M. Fan, Z.H. Liang, P.D. Han, Computation Materials Science 61 (2012) 180–184.
[18] L.J. Zhao, X.C. Zhang, C.M. Fan, Z.H. Liang, P.D. Han, Physica B 407 (2012) 3364–3370.
[19] X.F. Chang, J. Huang, Q.Y. Tan, M. Wang, G.B. Ji, S.B. Deng, G. Yu, Catalysis Communications 10 (2009) 1957–1961.
[20] X.F. Chang, J. Huang, C. Cheng, Q. Sui, W. Sha, G.B. Ji, S.B. Deng, G. Yu, Catalysis Communications 11 (2010) 460–464.
[21] F. Chen, H.Q. Liu, S. Bagwasi, X.X. Shen, J.L. Zhang, Journal of Photochemistry and Photobiology A: Chemistry 215 (2010) 76–80.
[22] S.Y. Chai, Y.J. Kima, M.H. Jung, A.K. Chakraborty, D. Jung, W.I. Lee, Journal of Catalysis 262 (2009) 144–149.
[23] S. Shamaila, A.K.L. Sajjad, F. Chen, J.L. Zhang, Journal of Colloid and Interface Science 356 (2011) 465–472.
[24] H.F. Cheng, B.B. Huang, X.Y. Qin, X.Y. Zhang, Y. Dai, Chemical Communications 48 (2012) 97–99.
[25] L. Zhang, W.Z. Wang, L. Zhou, M. Shang, S.M. Sun, Applied Catalysis B: Environmental 90 (2009) 458–462.
[26] B.F. Gao, A.K. Chakraborty, J.M. Yang, W.I. Lee, Bulletin of the Korean Chemical Society 31 (2010) 1941–1944.
[27] A.K. Chakraborty, S.B. Rawal, S.Y. Han, S.Y. Chai, W.I. Lee, Applied Catalysis A: General 407 (2011) 217–223.
[28] S. Shenawi-Khalil, V. Uvarovb, E. Menesa, I. Popovb, Y. Sasson, Applied Catalysis A: General 413–414 (2012) 1–9.
[29] F. Dong, Y.J. Sun, M. Fu, Z.B. Wu, S.C. Lee, Journal of Hazardous Materials 219-220 (2012) 26–34.
[30] B.C. Cao, P.Y. Dong, S. Cao, Y.H. Wang, Journal of the American Ceramic Society (2012), http://dx.doi.org/10.1111/jace.12073.
[31] C.L. Yu, F.F. Cao, Q. Shu, Y.L. Bao, Z.P. Xie, J.C. Yu, K. Yang, Acta Physico-Chimica Sinica 28 (2012) 647–653.
[32] P.Q. Wang, Y. Bai, J.Y. Liu, Z. Fan, Y.Q. Hu, Micro & Nano Letters 7 (2012) 876–879.
[33] S. Shenawi-Khalil, V. Uvarov, S. Fronton, I. Popov, Y. Sasson, Applied Catalysis B: Environmental 117–118 (2012) 148–155.
[34] B. Parea, B. Sarwana, S.B. Jonnalagadda, Applied Surface Science 258 (2011) 247–253.
[35] X.C. Zhang, L.J. Zhao, C.M. Fan, Z.H. Liang, P.D. Han, Physica B 407 (2012) 4416–4424.
[36] X.T. Shen, L.H. Zhu, H.W. Yu, H.Q. Tang, S.S. Liu, W.Y. Li, New Journal of Chemistry 33 (2009) 1673–1679.
[37] S.H. Cao, C.F. Guo, Y. Lv, Y.J. Guo, Q. Liu, Nanotechnology 20 (2009) 275702–275708.
[38] X.X. Liu, C.M. Fan, Y.F. Wang, Y.W. Wang, X.C. Zhang, Z.H. Liang, Science China Chemistry 55 (2012) 2438–2444.
[39] APHA, Standard Methods for the Examination of Water and Wastewater, 21st ed., APHA (American Public Health Association), American Water Works Association, and Water Pollution Control Federation, APHA, Washington, 2005, pp. 5–16 to 5–17, 5220C.
[40] M.D. Segall, P.L.D. Lindan, M.J. Probert, P.J. Hasnip, S.J. Clark, M.C. Payne, Journal of Physics: Condensed Matter 14 (2002) 2717–2744.
[41] J.P. Perdew, K. Burke, M. Ernzerhof, Physical Review Letters 77 (1996) 3865–3868.
[42] H.J. Monkhorst, J.D. Pack, Physical Review B 13 (1976) 5188–5192.
[43] Z.K. Cui, L.W. Mi, D.W. Zeng, Journal of Alloys and Compounds 549 (2013) 70–76.
[44] H.J. Zhang, L. Liu, Z. Zhou, RSC Advances 2 (2012) 9224–9229.
[45] H. Wang, X.F. Lang, J. Gao, W. Liu, D. Wu, Y.M. Wu, L. Guo, J.H. Li, Chemistry: A European Journal 18 (2012) 4620–4626.
[46] C.B. Cao, R.T. Lv, H.S. Zhu, Journal of Metastable and Nanocrystalline Materials 23 (2005) 79–82.
[47] H.L. Peng, C.K. Chan, S. Meister, X.F. Zhang, Y. Cui, Chemistry of Materials 21 (2009) 247–252.
[48] M. Qamara, Z.H. Yamani, Applied Catalysis A: General 439–440 (2012) 187–191.
[49] L. Zhou, W.Z. Wang, L.S. Zhang, H.L. Xu, W. Zhu, Journal of Physical Chemistry C 111 (2007) 13659–13664.
[50] Y.J. Zang, R. Farnood, Applied Catalysis B: Environmental 79 (2008) 334–340.
[51] Y.L. Pang, A.Z. Abdullah, Applied Catalysis B: Environmental 129 (2013) 473–481.
[52] A. Srikhaow, S.M. Smith, Applied Catalysis B: Environmental 130–131 (2013) 84–92.
[53] W.L. Huang, Q.S. Zhu, Computation Materials Science 43 (2008) 1101–1108.
[54] W.L. Huang, Q.S. Zhu, Journal of Computational Chemistry 30 (2009) 1882–1891.
[55] R.W. Godby, M. Schluter, L.J. Sham, Physical Review B 37 (1988) 10159–10175.
[56] H. Ariga, T. Taniike, H. Morikawa, M. Tada, B.K. Min, K. Watanabe, Y. Matsumoto, S. Ikeda, K. Saiki, Y. Iwasawa, Journal of the American Chemical Society 131 (2009) 14670–14672.
[57] B. Klahr, S. Gimenez, F. Fabregat-Santiago, T. Hamann, J. Bisquert, Journal of the American Chemical Society 134 (2012) 4294–4302.